PREDICTION OF MACROSCOPIC MULTIAXIAL BEHAVIOUR FROM MICROSTRUCTURAL OBSERVATIONS

G. Cailletaud, V. Doquet and A. Pineau
Centre des Matériaux - Ecole des Mines
B.P.87 - 9100 Evry Cédex (France)
UA CNRS N°866

Third International Conference on Biaxial/Multiaxial Fatigue
April 3-6, 1989, Stuttgart, F.R.G.

ABSTRACT

In this paper the effect of nonproportional loading on the cyclic behaviour of various materials is first reviewed. An attempt is made to analyse the influence of microstructural features on the amount of extra-hardening observed for complex out-of-phase loading. In particular the infuence of the stacking fault energy in FCC materials and the interaction mode between dislocations and precipitates is emphasized.

Then, experimental results obtained on 316L stainless steel are given. Tubular specimens were subjected to combined tension and torsion tests with various values of the λ' ratio ($\lambda' = \Delta\gamma/\Delta\epsilon$). Microstructural observations were made by SEM and TEM. The number of slip planes activated per grain was measured and the dislocation substructures analysed. The extra hardening observed in 316L stainless steel - especially for λ' values near $\sqrt{3}$ - is related to both an increase in slip activity and the formation of abundant mechanical microtwins.

A micro-macro model in which the crystallography (grains and slip systems) is introduced allows numerical simulations of the tests performed. Phenomenological variables are used to describe the hardening on each slip system. The predictions of the model are compared to both the mechanical results and the microstructural observations.

INTRODUCTION

The effect of nonproportional loading on the cyclic behaviour of various materials

Multiaxial low cycle fatigue has been intensively investigated during the last past decade. Large amounts of results dealing with extra hardening effects induced by non proportional loadings have been published (see e.g. [1,2]).

As far as modelling is concerned one may distinguish on the one hand, a "curve-fitting approach" based upon non-proportionality factors (Kanazawa et al [3], Ohnami et al[4]) and incremental plasticity approaches

using Mroz or memory surfaces models (Benallal and Marquis [5], Megahed [6] and McDowell [7]), on the other hand. Though, except Nishino et al [8], Clavel et al [9] and McDowell et al [10] who performed TEM observations, very few authors tried to elucidate the microstructural mechanisms of additional hardening. The explanation often proposed for this phenomenon - i.e. the raising of internal stresses by strong interactions between the numerous slip systems activated because of the principle axes rotation - is only qualitative.

From a compiling of data taken in the literature [3, 11-16] we will first try to draw general rules on the influence of certain microstructural features on the occurrence - or absence - of additional hardening.

The cyclic behaviour of various materials for a given plastic strain amplitude (i.e. $\Delta\epsilon p_{eq\ Mises} = 0.5\%$) is reported in Table 1. The uniaxial cyclic stress amplitude is compared to the monotonic tensile response and the amount of additional hardening observed for 90° out-of-phase loading above the uniaxial stress amplitude is given.

The examples of mild steel, copper (S.F.E. $\simeq$ 50 mJ/m^2) and 316L stainless steel (S.F.E. $\simeq$ 25 mJ/m^2) presenting 22, 33 and 73% additional hardening respectively indicate that the main parameter governing solid solutions work hardening is the degree of ease in cross slip. Temperature may be expected to have a large influence as well.

Then the uniaxial cyclic behaviour also has to be considered. "Strong" materials - whose ratio UTS/$\sigma_{0.2\%}$ is, according to a classical engineering rule smaller than or equal to 1.2 - are prone to cyclic softening under uniaxial loading. This tendency seems to be enhanced under out-of-phase loading since it counteracts the hardening effect of multiple slip activity thus giving rise to null (12% Cr steel) or weak hardening (1% Cr-Mo-V steel). On the other hand, strong additional hardening has to be expected under out-of-phase loading for "soft" materials - U.T.S./$\sigma_{0.2\%} \geqslant$ 1.4 - provided that they are solid solutions or contain unshearable precipitates such as 316L stainless steel, Waspaloy containing large γ' particles, and that their "cyclic hardening potential" is not almost exhausted under uniaxial cyclic loading - cf copper -.

As concerns precipitation-hardened materials whose precipitates are shearable, the hardening of the maxtrix may counterbalance the softening due to particle shearing - see e.g. Alloy 718 - or even exceeds it as is the case for Waspaloy which contains small γ' but has a U.T.S./$\sigma_{0.2\%}$ ratio equal to 1.57.

The present study, devoted to 316L stainless steel whose cyclic behaviour has proved very sensitive to nonproportionality and for which many data are available, has three principal aims : (i) investigate the effect of the $\lambda' = \Delta\gamma/\Delta\epsilon$ ratio on the multiaxial stress response of the material. (ii) contribute to the understanding of the micromechanisms of extra hardening. (iii) incorporate these micromechanisms into a numerical model in order to predict the macroscopic behaviour of FCC materials submitted to any loading path.

Material and experimental procedure

The chemical composition and the mechanical properties of the 316L steel investigated are given in Tables 2 and 3. A 30 mn annealing treatment performed at 1050C° under argon, followed by furnace cooling produced an average grain size of 50 μm. The specimens geometry and surface preparation are described elsewhere [13] where the details of experimental procedures and the definition of equivalent amplitudes are also given. The program of the uniaxial, multiaxial and sequential tests performed is sumed up in Table 4. Some test results are also taken from ref. [17] and [18].

Results and Discussion

A) Mechanical results

The cyclic stress response of the material is shown in Fig.1 together with the monotonic tensile curve using Von Mises equivalent amplitudes - although Tresca type equivalents fit better both the tension and torsion cyclic stress-strain curves -. It can be observed that, for a given equivalent plastic strain amplitude, the amount of additional hardening occurring under 90° out-of-phase loading is governed by the λ' ratio : for test IN1 ($\lambda' = 1.8$) it is twice that of test IN3 ($\lambda' = 5.4$) and 1.8 times that of a test taken from ref. [18] for which $\lambda' = 0.5$.

In order to specify to what extent this additional hardening is reversible, sequential tests - first 90° out-of-phase tension and torsion with $\lambda' = 1.8$ and second, tension-compression with an imposed plastic strain amplitude - were performed (see Table 4). The variations of the equivalent stress range during these sequences are drawn in Fig.2, together with the stress range obtained at the second level without prior straining. As loading becomes proportional the material softens very quickly but, when failure occurs, the stress range still exceeds the reference value by 20% for test IN8 and by 30% for test IN6.

These results are to be compared to pure tension sequential tests results for the same material [19] . After stabilization under a large strain amplitude, the strain memory evanescence at the second level was slow and never complete (Fig.3).

B) Microstructural observations

SEM observations of specimens outer free surface show that nonproportional loading generates more homogeneous slip activity from one grain to another than proportional loading does (Fig.4). Each grain is actually more likely to take part to plasticity when the principle axes turn than when the directions of maximum shear strain have a fixed direction with respect to its crystallographic orientation.

This is consistent with McDowell et al's observation on a type 304

stainless steel : nonproportional loadings generate a more homogeneous distribution of deformation products (i.e. α' martensite) [10]. Moreover, surface rumpling is more pronounced for specimen submitted to out-of-phase loading and slip lines seem to be somewhat wavy. To quantify the multiplicity of slip responsible for extra-hardening effects, the average number of activated slip planes per grain and the mean distance between intense shear bands of the same orientation were measured on the outer surface of specimens (Table 5). Despite an important scatter it can be concluded that, for a given equivalent strain range, non-proportional loadings increase both the number of activated slip systems - the number of traces per grain reaches 1.9 for test IN3 whereas it is only 1.25 for the equivalent tension test IN4 - and the mean distance between the intense slip lines. It is worth noting that this distance increases with the equivalent stress response obtained, as if the strain localization became more and more difficult as the matrix hardens. The two results are consistent with similar observations by Clavel et al [9] for Waspaloy.

TEM observations revealed only ladders, veins or dislocation cell structures with loose outlines in specimens submitted to uniaxial tests, but walls, cells and above all, abundant microtwining for specimens IN3 and IN1 (Fig.3).In the latter case the critical shear stress needed to induce twining has been reached because of extra-hardening. The average size of dislocation cells has been measured for three specimens (Table 5). As usually observed it decreases with increasing equivalent stress range.

The persistence of a certain strain memory effect observed during sequential tests is thus related to the permanence of mechanical twins whereas the softening following the load variation is due to the rearrangement of dislocations into cells whose size corresponds to the second strain level.

Modelling

Introduction

Two different scales of inhomogeneity have to be considered when dealing with the deformation of a polycrystal.

The first one is associated with strain incompatibilities between adjacent grains. These are responsible for local stresses that differ from the macroscopic stress. The resulting intergranular hardening is described in the model through a simplified self-consistent scheme leading to kinematic intergranular hardening. Neither the grain geometry nor its location is specified.

The second one takes place within the grains. In the model the local geometry, for instance, the existence of more or less deformed zones inside the grain, are not taken into account. The hardening of each slip system is represented by a partly reversible component, which is the kinematical variable, and by an irreversible term, which is the isotropic

variable. The former relates to long distance interactions such as dislocations loops left around unshearable precipitates [20] or dislocations walls [21]. The latter corresponds to short range interactions such as friction stresses due to particule shearing or dislocation interactions.

Presentation of the model

The model used in this section has already been described and applied to 316L stainless steel [22], [23]. Only a short account is given here. The model is expressed in the framework of viscoplasticity. As previously explained, several levels are involved in the constitutive equations (Fig.6). The viscoplastic character is only present in the relations written at the microlevel, so that slip indetermination is avoided. Two main branches are considered in the diagram :

- The "localization" process is the "micro-going-branch"; including first the relation between the macroscopic variables (stress and viscoplastic strain tensors : $\tilde{\Sigma}$ and $\tilde{E}_v$), and the corresponding ones in each grain g ($\tilde{\sigma}^g$ and $\tilde{\epsilon}^g_v$). A simple linear combination is used, with a material coefficient A accounting for local strain incompatibilities :

$$\tilde{\sigma}^g = \tilde{\Sigma} + A\ (\tilde{E}_v - \tilde{\epsilon}^g_v) \qquad (1)$$

The second step gives the resolved shear stress τ^s on each system s through a projection of the local stress with the orientation tensor $\tilde{m}^s$:

$$\tau^s = \tilde{\sigma}^g : \tilde{m}^s \qquad (2)$$

- the "homogenization process" corresponds to the "macro-going-branch". The viscoplastic strain rate tensor $\dot{\tilde{\epsilon}}^g_v$ of each grain has first to be calculated from the viscoplastic shear strain rate $\dot{\gamma}^s$ on each system s. The macroscopic strain rate tensor $\dot{\tilde{E}}_v$ results from the summation of the $\dot{\tilde{\epsilon}}^g_v$ values.

In the constitutive equations written on a microscale for each system, the viscoplastic shear strain rate is defined as a power function of the effective stress obtained by the difference between the resolved shear stress and the hardening variables x^s and r^s on the system s :

$$\dot{\gamma}^s_v = \left\langle \frac{|r^s - x^s| - r^s}{k} \right\rangle^n \text{sign}\ |\tau^s - x^s| \qquad (3)$$

with $\langle H \rangle$ = positive part of H.

The variable r^s represents the isotropic component of the hardening while x^s corresponds to its kinematic part. A non linear kinematic

evolution is used for x^s and an exponential function, which saturates as the cumulated viscoplastic shear strain increases, describes the variation of r^s:

$$\dot{x}^s = c\,\dot{\gamma}_v^s - d\,x^s\left|\dot{\gamma}_v^s\right| \tag{4}$$

$$\dot{r}^s = \sum_{j \in G} bQ\,h_{sj}\exp(-b\,v^j)\,.\,\left|\dot{\gamma}_v^j\right| \tag{5a}$$

$$\text{with } v^j(t) = \int_o^t \left|\dot{\gamma}_v^j(r)\right| dr \tag{5b}$$

In the preceding equations, seven material coefficients are used. One of them defines the intergranular hardening (A in Eq.(1)). The other ones account for intragranular hardening (c, d, b, Q in (4) and (5)), and for viscosity (K and n in eq.(3)). The initial value of r^s is denoted by r_o. Cross hardening is given by the coefficients h_{rs} of the interaction matrix. Only octahedral slip is taken into account so that the interaction matrix is reduced to 12 by 12. Its form is shown in Fig.7. We used here the Taylor's assumption of isotropic interaction implying that $h_1 = h_2 = h_3 = h_4 = 1$.

Identification for 316L stainless steel

The simulations were performed using two populations of grains, issued from Ref. [23,25]. They were chosen such as to represent polycrystal as isotropic as possible. The material coefficients are given in Table 6.

The initial value of the isotropic variable controls the onset of plastic deformation on each glide system. Both intergranular and intragranular hardening influence the transient shape of the hysteresis loop. Intergranular hardening is predominant for low values of accumulated plastic strains and quickly reaches saturation[26]. It is worth noting that, unlike in classical macroscopic models, the asymptotic value of the isotropic component is sensitive to the loading path.

Fig. 8 shows an example of the resulting stress path calculated for test IN1. Note that the saturation rate is increased in the simulation in order to save CPU time.The longitudinal and shear stress ranges predicted by the model for a given equivalent strain range - $\Delta\varepsilon_{eq}/2 = 0.5\%$ - are plotted as a function of the λ' ratio together with the measured values in Fig. 9. The agreement between calculated and measured stress responses is good, especially for intermediate λ' values. These simulations showed that the value of the intergranular hardening component measured by the mean difference between local and global stresses remains very low ($\simeq$ 20 to 30 MPa). It was also observed that for both uniaxial and complex loading, the kinematic transgranular hardening is of the order of 80 MPa. This macroscopic value is assessed by using a Taylor factor of 3. Therefore the main contribution to hardening arises from the isotropic component. Typically the local isotropic hardening component r^s was found to reach

values of ≃ 120 MPa and ≃ 220 MPa for IN4 and IN1, respectively. This significant increase in the isotropic hardening traduces the decrease in cell size and the formation of mechanical twins (Table 5).

The model also allows an analysis of slip activity in each grain, represented as an unfolded Thompson tetrahedron (Fig.10a and 10b). The comparison between these figures illustrates the ability of the model to reproduce the increase in slip activity induced by nonproportional loadings.

Histograms were drawn, showing the percentage of grains - among those taking part to plasticity - in which 1, 2, 3 or 4 slip planes contain at least one system whose accumulated viscoplastic strain, $\gamma^{\cdot}_{v,cum}$ exceeds a given threshold $\gamma^{th}_{v,cum}$. These frequencies are compared to the measured frequencies of grains showing a unique, double or triple set of slip line traces at the outer surface of the specimens (Fig.11). The agreement between the calculated and measured frequencies is good provided one considers a threshold of 1% cumulated strain for the uniaxial test and 4% for the out-of-phase test.

This difference might arise from inherent experimental scatter or from the model which is still at a development stage. Up to now the memory of the previous strain path is permanent, so that the partial softening effect observed during sequential tests cannot be represented. In the same way, the number of slip systems activated under out-of-phase loading is probably overestimated. Further research has to be made notably to compare slip activity for tension and torsion. The presence of two distinct phenomena at the microstrutural level - ie cells and twins formation - suggests to use a more complex interaction model between slip systems, including a fully irreversible term and a partly reversible one [27].

CONCLUSIONS

- The degree of ease in cross slip, the initial "hardenability" of a material - expressed by the ratio $UTS/\sigma_{o.2\%}$-, the shearability of hardening precipitates were shown to be material features that govern the amount of hardening under non-proportional multiaxial loading.

- The influence of a mechanical parameter, ie the ratio λ' of shear to axial strain amplitudes, was also specified.

- The deformation substructures resulting from out-of-phase loadings in 316 stainless steel were observed. Additional hardening was shown to be related to both an increase in slip activity and the formation of mechanical microtwins.

- A rather satisfactory attempt of micro-macro modelling was made; The model was found able to predict accurately enough both the extra hardening and the degree of multiplicity of slip observed under nonproportional loadings.

References

[1] "Multiaxial Fatigue" A.S.T.M. STP 853 Miller/Brown, Editors, August 1985.

[2] Second International Conference on Biaxial/Multiaxial Fatigue, 16-20 déc. 1985. Sheffield University.

[3] Kanazawa, K., Miller, K.J. and Brown, M.W., "Cyclic deformation of 1% CrMoV, Steel under out of phase loads" Fat. of Eng. Mat. and Struc., vol.2, 1979, pp.217-28.

[4] Ohnami, M., Sakane, M., Nishino, S., "Cyclic behavior of a type 304 stainless steel in biaxial stress states at elevated temperatures". Int. Jour. of Plast., vol.4, 1988, pp.77-89.

[5] Benallal, A., Marquis, D., "Constitutive equations for non-proportional cyclic elasto-visco-plasticity". Journ. of Eng. Mat. and Tech. vol.109, 1987, pp.326-36.

[6] Megahed, M. "A critical examination of nesting, bounding and memory surfaces plasticity theories under non-proportional loading conditions". Journ. of Mech. Sci. vol.30, n°2, 1988, pp.101-18.

[7] McDowell, D.L. "An experimental study of the structure of constitutive equations for non-proportional cyclic plasticity", Journ. of Eng. Mat. and Tech., vol.107, 1985, pp.307-15.

[8] Nishino, S., Hamada, N., Sakane, M., Ohnami, M., Matsumara, N., Tokizane, M. "Microstructural study of cyclic strain hardening behaviour in biaxial stress states at elevated temperatures". Fat. and Fract. of Eng. Mat. and Struc., vol.9, n°1, 1986, pp.65-77.

[9] Clavel, M., Pilvin, P., Rahouadj, R. "Plasticité cyclique sous sollicitations non proportionnelles", Mémoires et Etudes Scientifiques Revue de Métallurgie, Sept.88, p.457.

[10] McDowell, D.L., Stahl,D.R., Stock, S.R., Antolovitch, S.D. "Biaxial path dependence of deformation substructure of type 304 stainless steel", Met. Trans. vol.19A, 1988, pp.1277-93.

[11] Locicéro, R., Pineau, A., Work in progress at the Centre des Matériaux - Ecole des Mines de Paris, France.

[12] Robillard, M., Cailletaud, G. "Directionally defined damage in multiaxial low cycle fatigue : experimental evidence and tentative modelling". This volume.

[13] Doquet, V. Pineau, A. "Multiaxial low cycle fatigue behaviour of a mild steel". This volume.

[14] Fatemi, A., Socie, D.F. "A critical plane approach to multiaxial fatigue damage including out-of-phase loading". Fat. Fract. Eng. Mat. Struct., vol.11, n°3, 1988, pp.149-65.

[15] McDowell, D.L., Socie, D.F., Lamba, H.S. "Multiaxial non proportional cyclic deformation". Low cycle fatigue and life prediction ASTM-STP 770, 1982, pp.500-518.

[16] Koch. J.L. "Proportional and non proportional biaxial fatigue of Inconel 718". Report 121, Mat. Eng. Mech. Beh. College of Engineering, University of Illinois at Urbana Champaign, 1985.

[17] Jacquelin, B., Hourlier, F., Pineau, A. "Crack initiation under low cycle multiaxial fatigue". ASTM-STP 853, Multiaxial Fatigue, 1985, pp.285-313.

[18] Cailletaud, G., Kaczmarek, H., Policella, H. "Some elements on multiaxial behaviour of 316L stainless steel at room temperature". Mech. of Mat. vol.3, n°4, 1984, pp.333-47.

[19] Nouailhas, D., Cailletaud, G., Policella, H., Marquis, D., Dufailly, J., Lieurade, H.P., Ribes, A., Bollinger, E. "On the description of cyclic hardening and initial cold working". Eng. Fract. Mech., vol.21, N°4, 1985, pp.887-95.

[20] Brown, L.M., Stobbs, W.M., "The work hardening of copper-silica. A model based on internal stresses with no plastic relaxation", Phil. Mag., vol.23, pp.1185-99, (1971).

[21] Mughrabi, H., "Dislocation wall and cell structures and long-range internal stresses in deformed metal crystals", Acta Met., vol/31, pp.1367-1379, (1983).

[22] Cailletaud, G., "Une approche micromécanique du comportement des polycristaux", Revue Phys. Appl. 23, pp.353-365, (1988).

[23] Cailletaud, G., "A micromechanical approach to inelastic behavior of metals, polycristal modeling", presented at ASME/SES Summer Annual meeting, Berkeley, June 1988.

[24] Cailletaud, G. "Une approche micromécanique phénoménologique du comportement inélastique des métaux", thèse Univ. Paris VI, (1987).

[25] Fortunier, R. "Deformation plastique de cristaux métalliques CFC" Thesis Ecole des Mines de Saint-Etienne, (1987).

[26] Berveiller, M., Zaoui, A., "An extension of the self-consistent scheme to plastically flowing polycrystals", J. Mech. Phys. Solids, vol.26, pp.325-344, (1979).

[27] Fer, F. "Thermodynamique macroscopique", Paris, Gordon et Breach ed. 1970.

	FCC materials					BCC materials			
	Precipitation hardened			Solid solutions		Tempered martensite	Tempered Bainite	Ferrite + pearlite	Ferrite
	Shearable precipitates		Unshearable precipitates						
Material	Waspaloy containing small γ' precipitates (Φ = 8 nm)	Alloy 718	Waspaloy containing large γ' precipitates (Φ = 90 nm)	Copper (SFE 50 mJ/m²)	316L stainless steel (SFE 25 mJ/m²)	12% Cr steel	1% CrMoV steel	1045 steel	Mild steel
UTS/$\sigma_{\varepsilon 0,2\%}$	1.57	1.2	1.7	3.4	2.1	1.2	1.2	1.75	1.42
$\frac{\sigma_{cyc}-\sigma_{mon.}}{\sigma_{mon.}}$ in tension at $\Delta\varepsilon_p$=0.5%	+1%	-16%	15%	+105%	+18%	-10%	softening	+21%	+29%
$\frac{\sigma^{90°}_{mult}-\sigma_{cyc}}{\sigma_{cyc}}$ at $\Delta\varepsilon^{Mises}_{eq}$=0.5%	+16%	0%	+35%	+33%	+73%	0%	+14%	+13%	+22%
Référence	[11]	[16]	[11]	[15]	this study	[12]	[3]	[14]	[13]

Table 1 - Uniaxial and multiaxial cyclic behaviour of several materials. σ_{mon}, σ_{cyc} and $\sigma^{90°}_{mult}$ stand respectively for the tensile stress at ϵ_p = 0,25%, the stabilized stress range under tension compression for $\Delta\epsilon_p$ = 0,5% and the Von Mises equivalent stress range obtained during 90° out-of-phase loading for an equivalent plastic strain range of 0.5%.

C	N	Ni	Cr	Mo	Mn	Cu	Si	Co	P	S
0.034	0.068	12.45	17.3	2.52	1.85	0.2	0.53	0.11	0.029	0.004

Table 2 - Chemical composition of 316L stainless steel (weight %).

0.2% proof stress (MPa)	U.T.S. (MPa)	Elongation (%)	E (MPa)	μ (MPa)
321	592	50	180000	68000

Table 3 - Mechanical properties of 316L stainless steel.

Test	λ'	φ (°)	$\Delta\varepsilon/2$ (%)	$\Delta\gamma/2$ (%)	$\Delta\sigma/2$ (MPa)	$\Delta\tau/2$ (MPa)	$\Delta\varepsilon_{eq}^{Mises}$ (%)	$\Delta\varepsilon_{eq}^{Mises}$ (%)	$\Delta\varepsilon_{eq}^{Mises}$ (MPa)	N, N_r (cycles)
IN4	0	0	0.53	0	308	0	0.53	0.38	308	2730(b)
TT5	∞	0	0	0.89	0	165	0.51	0.37	2.86	48000
IN7	1.8	90	0.33	0.59	425	234	0.35	0.22	430	4000
IN1	1.8	90	0.5	0.9	520	294	0.52	0.35	530	1612
IN2	0.9	90	0.51	0.47	488	260	0.50	0.29	480	2624
IN3	5.4	90	0.165	0.9	291	232	0.52	0.37	403	3818
IN6 part 1	1.8	90	0.5	0.9	517	271	0.55	0.38	517	1700(b)
IN6 part 2	0	0	(a)	0	(a)	0	(a)	0.23	(a)	3644
IN8 part 1	1.8	90	0.32	0.61	435	247	0.35	0.2	439	1700(b)
IN8 part 2	0	0	(a)	0	(a)	0	(a)	0.23	(a)	2925

(a) decreasing; (b) interrupted test.

Table 4 - Tests conditions and results.

Test	IN4 (λ' = 0)	IN2 (λ' = 0.9)	IN1 (λ' =1.8)	IN7 (λ' = 1.8)	IN3 (λ' = 5.4)	TT5 ($\lambda' \rightarrow \infty$)
number of traces per grain	1.25 (0.4)	1.6 (0.6)	1.7 (0.6)	1.5 (0.5)	1.9 (0.7)	-
mean distance between intense slip bands	3.1 µm (1.4)	4.7 µm (1.6)	5.5 µm (2.7)	4.05 µm (1.3)	4.3 µm (3.2)	-
mean diameter of cells	no definite cells	-	0.57 µm	-	0.68 µm	0.8 µm

Table 5 : Quantitative results of SEM and TEM observations. The numbers between brackets are standard deviations.

A (MPa)	r_o (MPa)	b -	Q (MPa)	n -	K ($MPa.s^{\frac{1}{n}}$)	c (MPa)	d -
2000	50	20	50	25	50	3000	100

Table 6 - Coefficients used for the simulations.

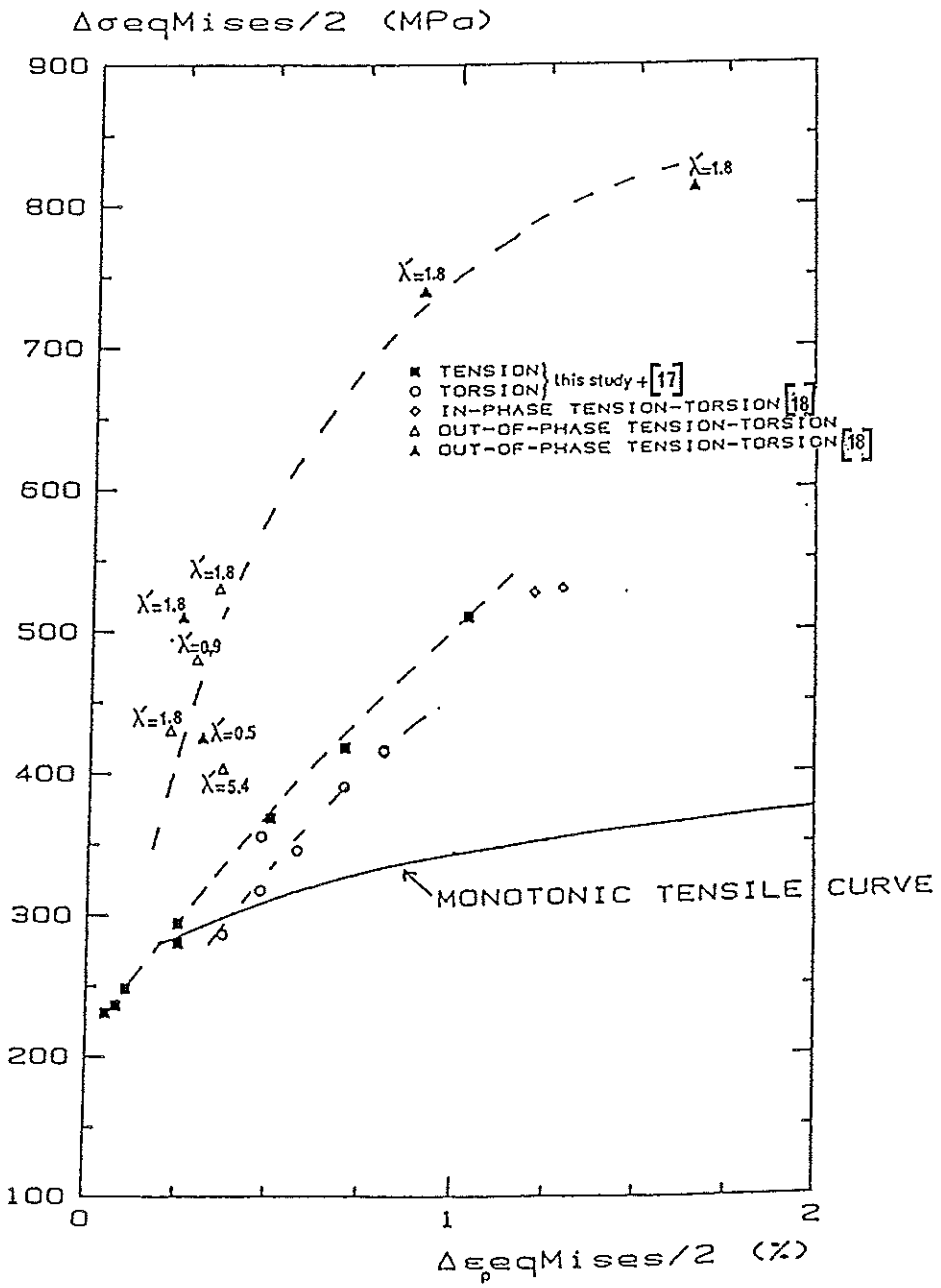

Fig. 1 - Uniaxial and multiaxial cyclic stress-strain curves using Von Mises equivalents.

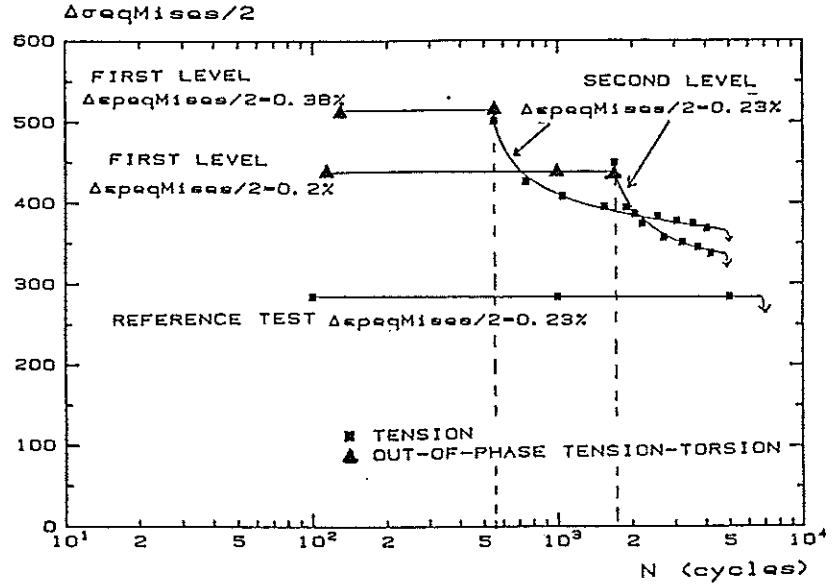

Fig. 2 - Evolution of the equivalent stress range during sequential tests. First part : out-of-phase tension and torsion, second part : tension-compression.

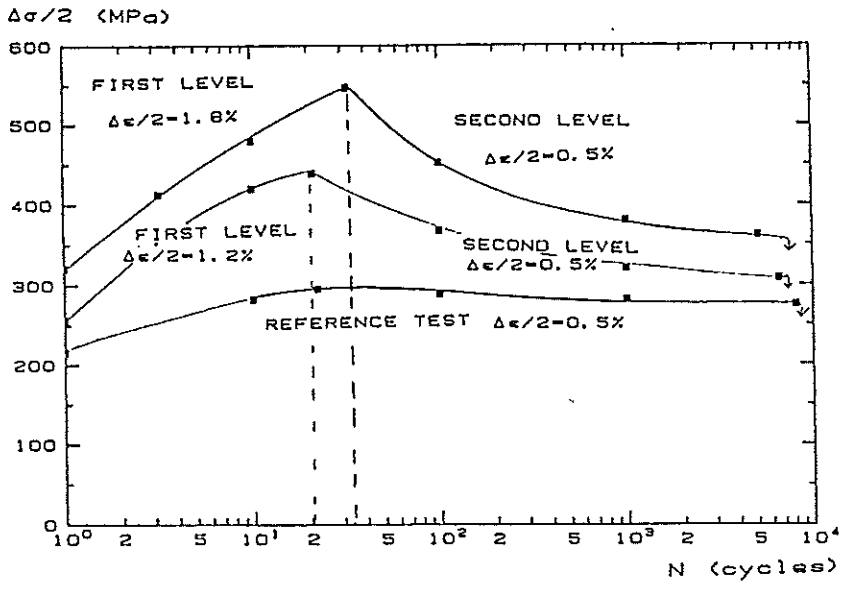

Fig. 3 - Evolution of the stress range during uniaxial sequential tests performed by Nouailhas et al [17] on 316L stainless steel.

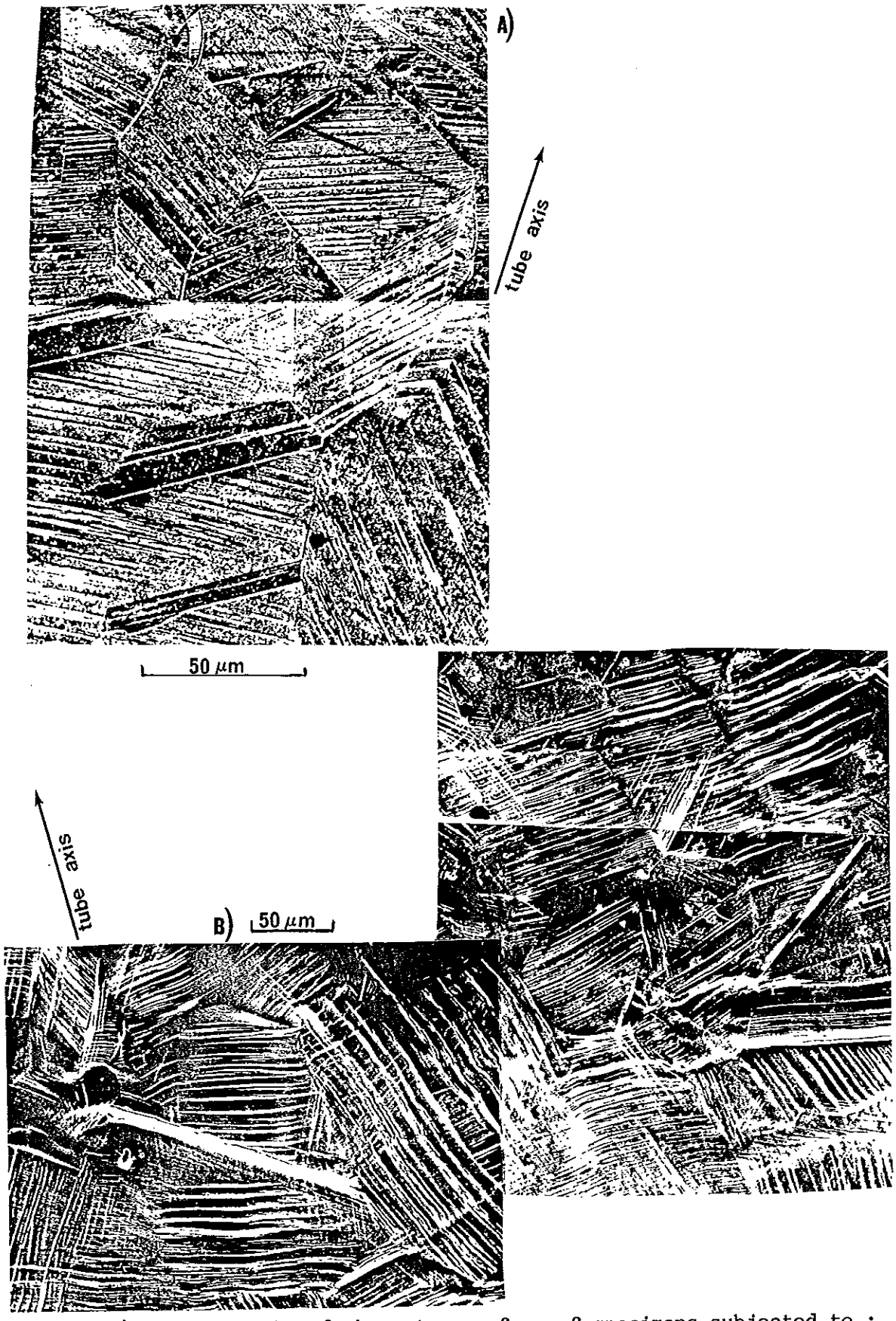

Fig. 4 - Micrographs of the outer surface of specimens subjected to :
a) tension-compression (test IN4);
b) out-of-phase tension and torsion (test IN1).

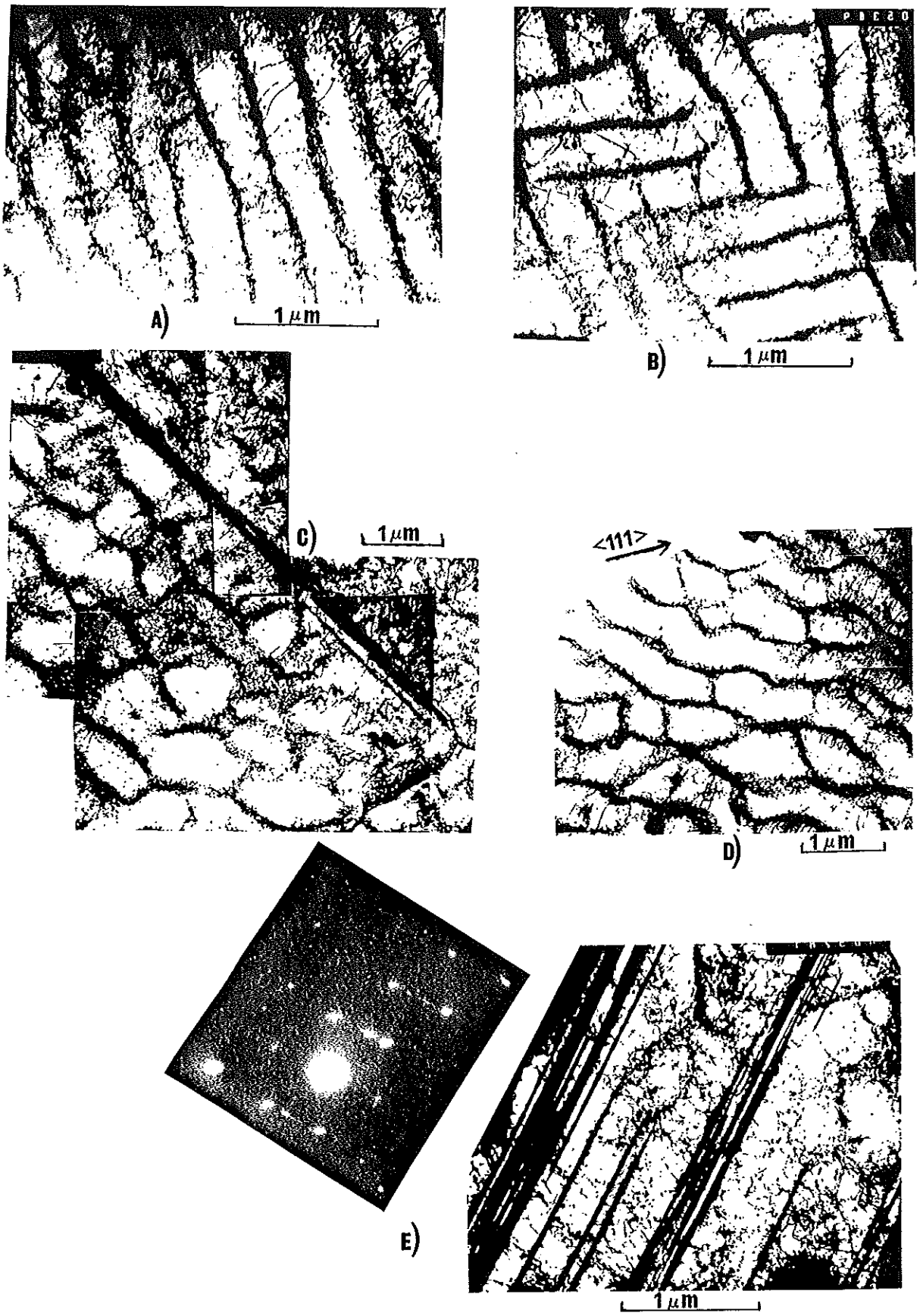

Fig. 5 - TEM observations of deformation substructures performed on specimens IN3) a) b) c) and IN1) d) e)

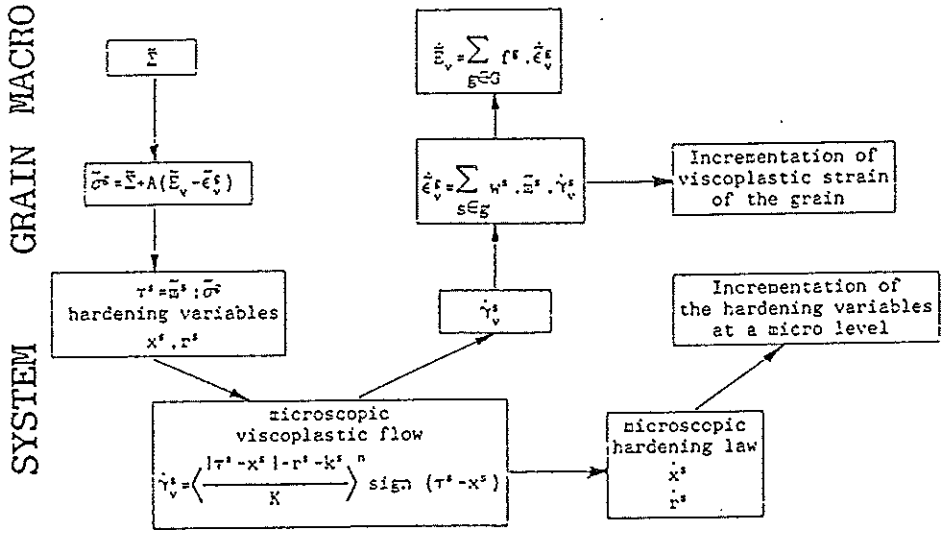

Fig. 6 - The three levels considered in the model.
(w^s and f^g are resp. volume fraction of active slip system in a family and volume fraction of grain of a given orientation : they are taken equal to 1 in the applications of this paper).

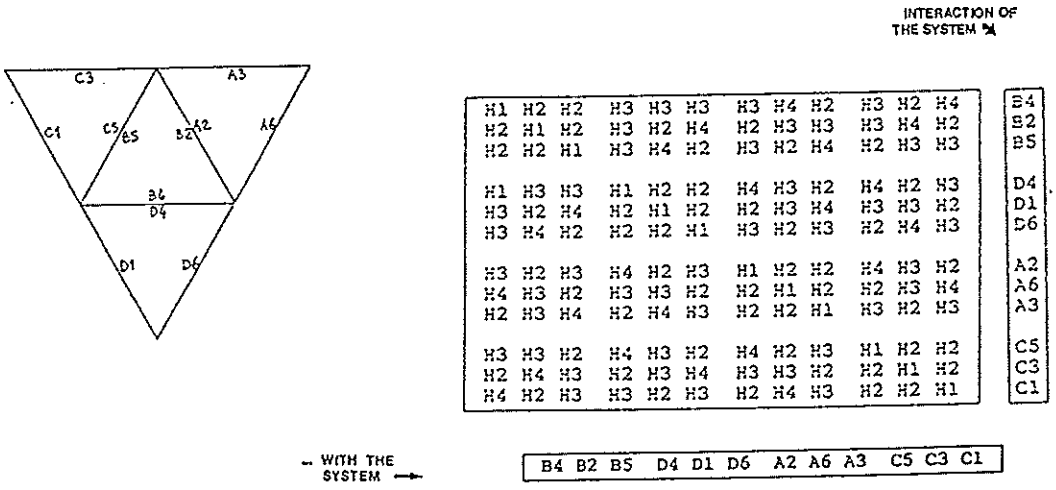

Fig. 7 - The shape of the interaction matrix.

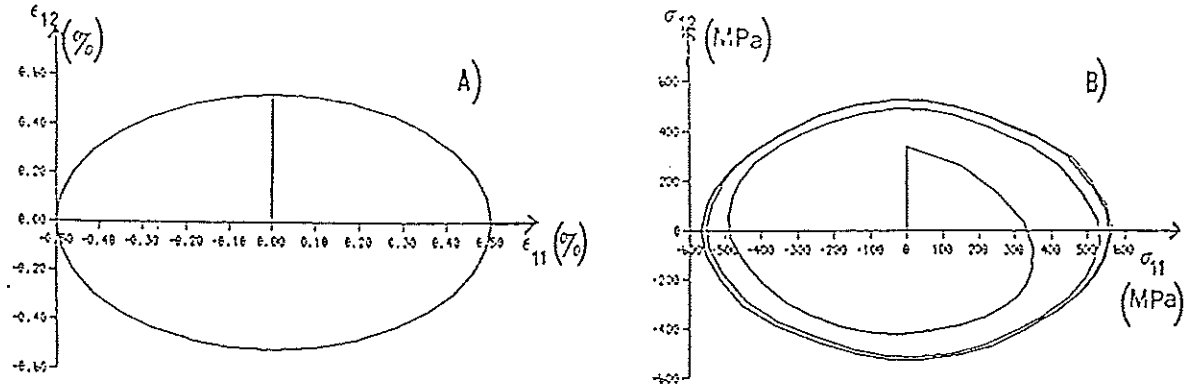

Fig. 8 - a) The simulated strain path; b) the predicted stress path.

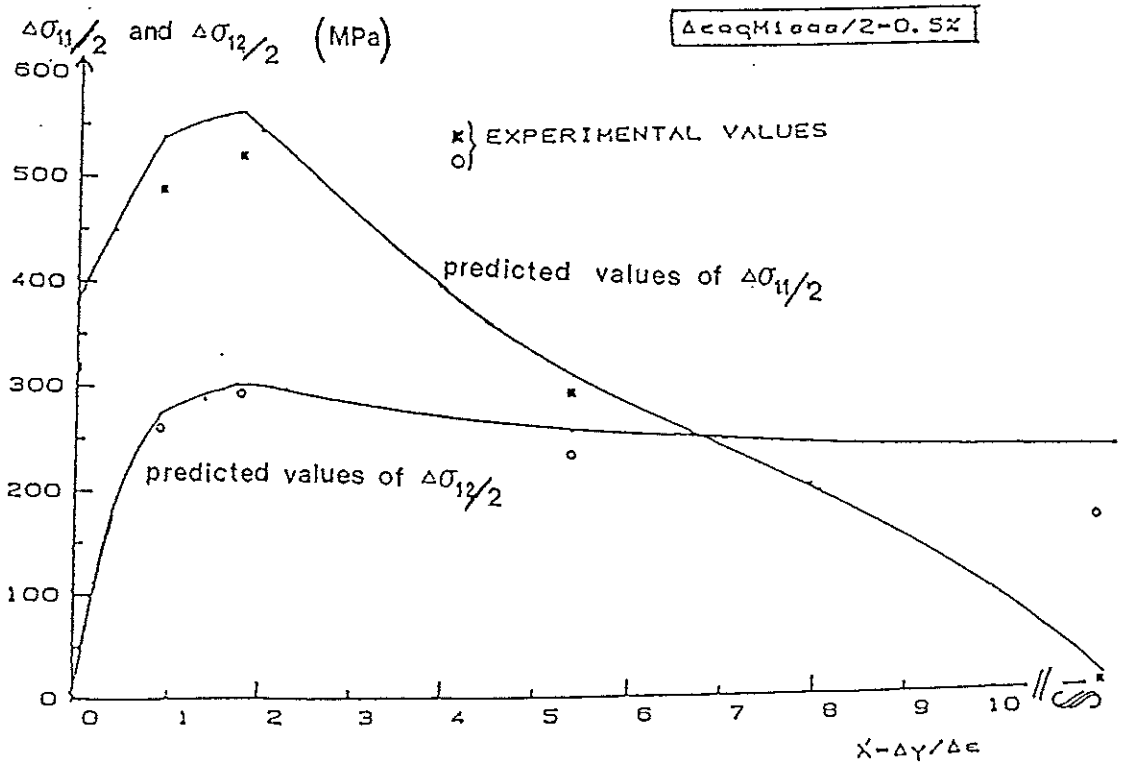

Fig. 9 - Comparison between predicted and experimental values of shear and axial stress ranges as a function of the λ' ratio.

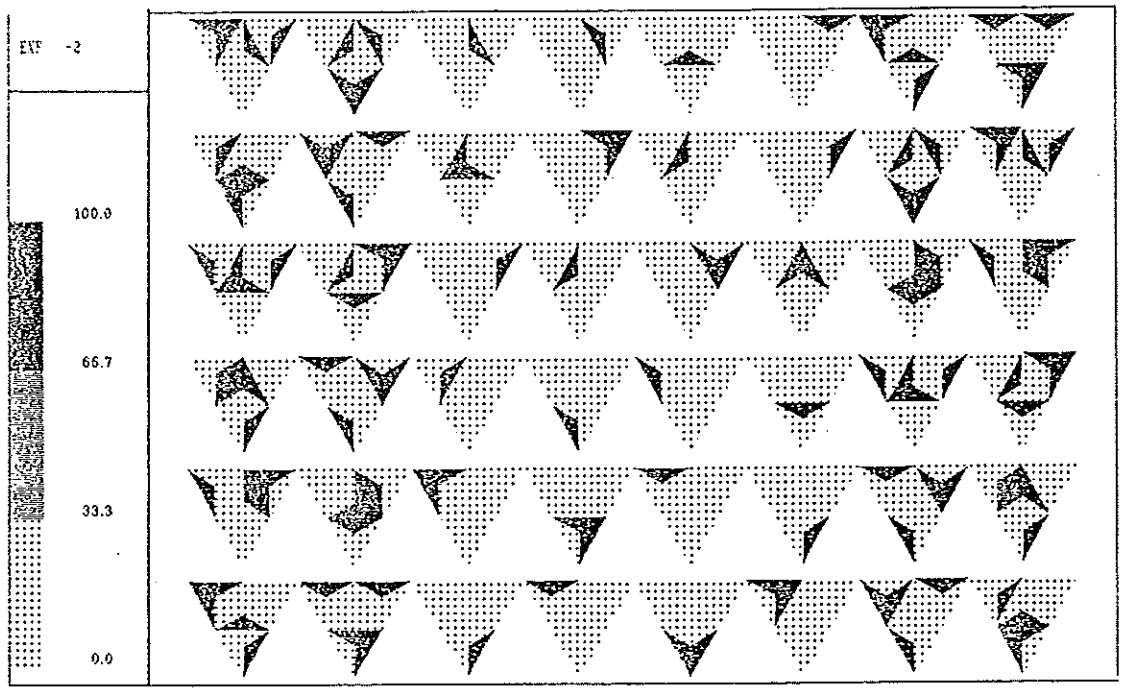

A)

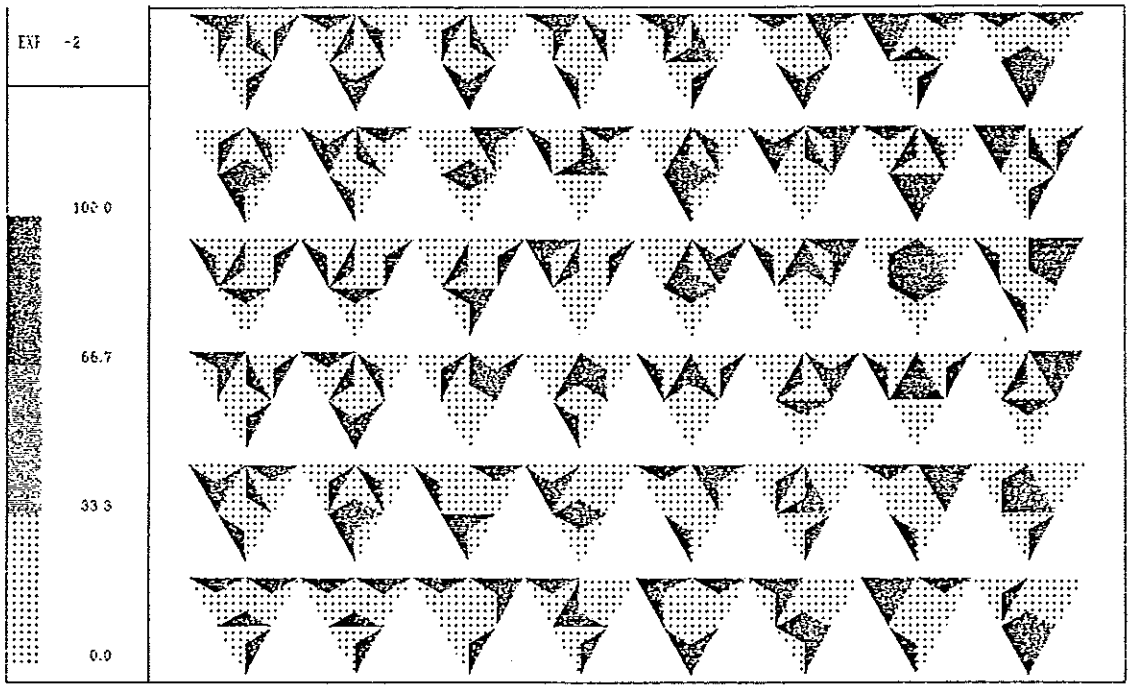

B)

Fig. 10

Slip systems having undergone a cumulated viscoplastic strain $\gamma_{v,cum}$ larger than 0.1% after,

a) 4 cycles under tension-compression,

b) 4 cycles under out-of-phase tension and torsion at the same equivalent strain range ($\lambda' = 1.8$).

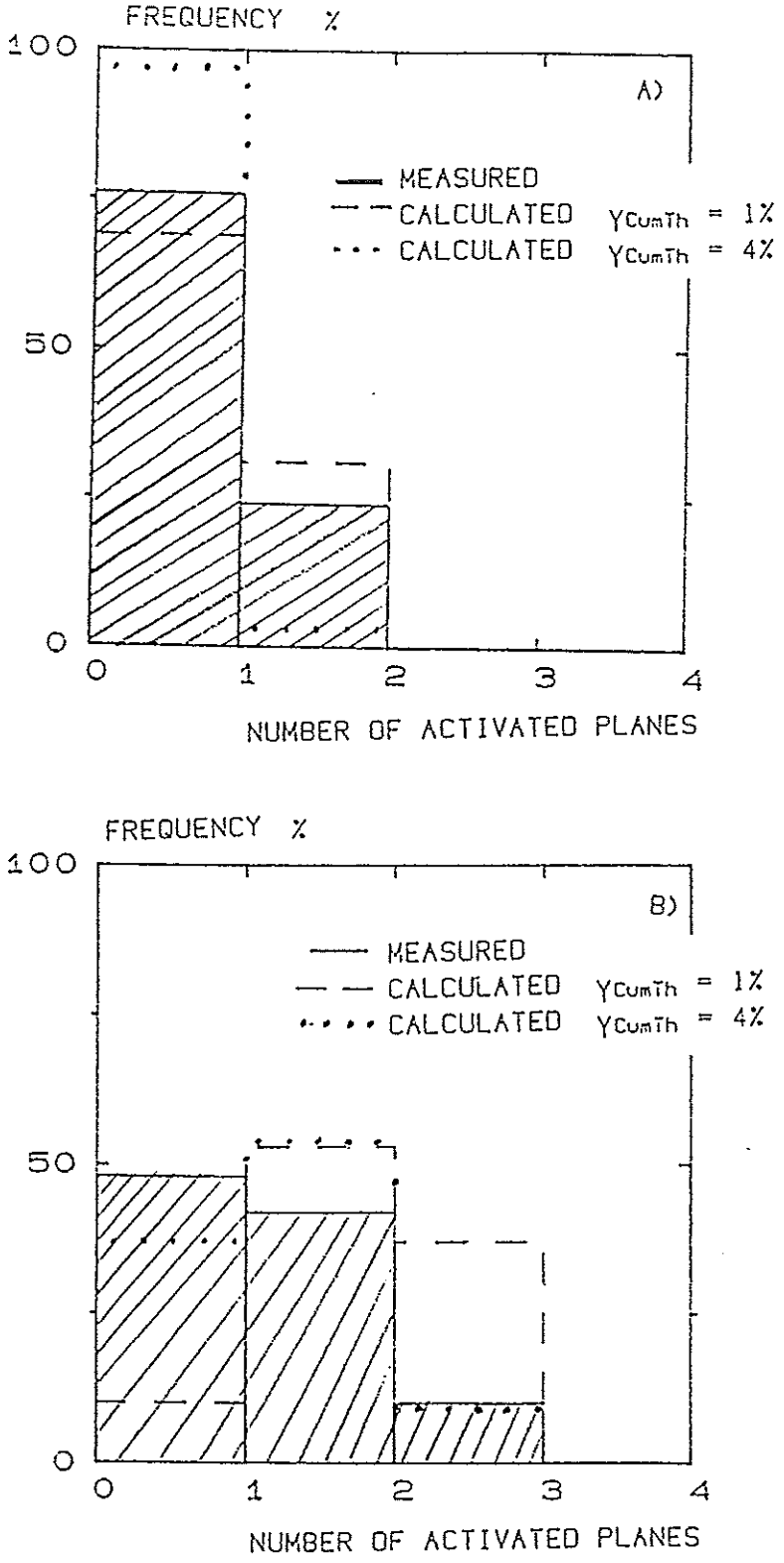

Fig. 11 - Calculated frequencies of plasticized grains in which 1, 2, 3 or 4 slip planes contain at least one system whose $\gamma^{s}_{v,cum}$ exeeds a given threshold $\gamma^{th}_{v,cum}$. a) simulation of test IN4, b) simulation of test IN1.